Electronic Supplementary Information

Polyoxometalate-Modulated Self-Assembly of Polystyrene-*block*-Poly(4-vinylpyridine)

Xiankun Lin,[a, §] Fang Liu,[a] Haolong Li,*[a] Yi Yan,[a] Lihua Bi,[a] Weifeng Bu,[b]

and Lixin Wu*[a]

[a]State Key Laboratory of Supramolecular Structure and Materials, Jilin University, Changchun 130012, P. R. China
[b]Key Laboratory of Nonferrous Metal Chemistry and Resources Utilization of Gansu Province, State Key Laboratory of Applied Organic Chemistry, and College of Chemistry and Chemical Engineering, Lanzhou University, Lanzhou 730000, P. R. China
[§]Present Addresses: Micro/Nano Technology Research Centre, Harbin Institute of Technology, Harbin 150080, P. R. China
*Corresponding Author: wulx@jlu.edu.cn (L. W.); hl_li@jlu.edu.cn (H. L.)

Materials.

The polystyrene-*block*-poly(4-vinylpyridine) (PS_{94}-*b*-$P4VP_{95}$, where the subscripts refer to the degree of polymerization) was purchased from Polymer Source Inc.. The polydispersity index of the copolymer is 1.09. Phosphotungstic acid ($H_3PW_{12}O_{40}$, denoted as HPW) and silicotungstic acid ($H_4SiW_{12}O_{40}$, denoted as HSiW) were purchased from Sinopharm Chemical Reagent Co. Ltd.. *N*,*N*-dimethylformamide (DMF) is of analytical grade.

Preparation of BC–POM composites.

First of all, the block copolymer PS_{94}-*b*-$P4VP_{95}$ and the chosen POM with a given molar ratio were dissolved in DMF, respectively. The DMF solution of POM was added dropwise into the copolymer solution under stirring at room temperature. The mixture solution was stirred for 20 min at least, and then the composite solution was standby for measurement. Unless otherwise noted, the final solutions were kept at a copolymer concentration of 1.0 mg/mL.

In the present study, DMF has been chosen as the solvent. The other choices THF and $CHCl_3$ are not suitable for the present study. Although both THF and $CHCl_3$ are also the common solvents for the polystyrene-*block*-poly(4-vinylpyridine), both HPW and HSiW have very low solubility in $CHCl_3$ and are prone to form the oil-like complexes with THF.

Characterization.

^{1}H NMR spectra were recorded on a Bruker Avance 500 instrument using DMF-d_7 as solvent and residual protons of DMF-d_7 as internal standard. Fourier transform infrared spectroscopy (FT-IR) spectra were carried out on a Bruker Optics VERTEX 80v FT-IR spectrometer equipped with a DTGS detector (32 scans) with a resolution of 4 cm^{-1} from pressed KBr pellets. Transmission electron microscopy (TEM) measurements were performed using a Hitachi H800 electron microscope operating at an accelerating voltage

of 200 KV. Several droplets of the composite solution were placed on a carbon-coated copper grid for about 1 min, following sucking by filter papers and drying at atmosphere pressure and room temperature. The aggregated structures of composites were investigated without staining due to the strong electron scattering by heavy atoms containing in POMs and the selective interaction between POMs and P4VP blocks. For the sample in which isolated micelles are difficult to observe, the sample was treated through shortening the time for which the composite solution was placed on a grid or rinsing the prepared copper grids with composites in pure tetrahydrofuran (THF) for several seconds to reduce non-absorbed composites.[1] High angle annular dark field scanning transmission electron microscopic (HAADF-STEM) images, energy-dispersive X-ray (EDX) spectra, and EDX elemental mapping were collected on a FEI Tecnai F20 microscope operating at an accelerating voltage of 200 KV. Scanning electron microscopic (SEM) images were collected on a JEOL JSM-6700F field emission scanning electron microscope and thin, cleaned Si wafers were employed as substrates.

Influence of POM charges on the micellar morphologies.

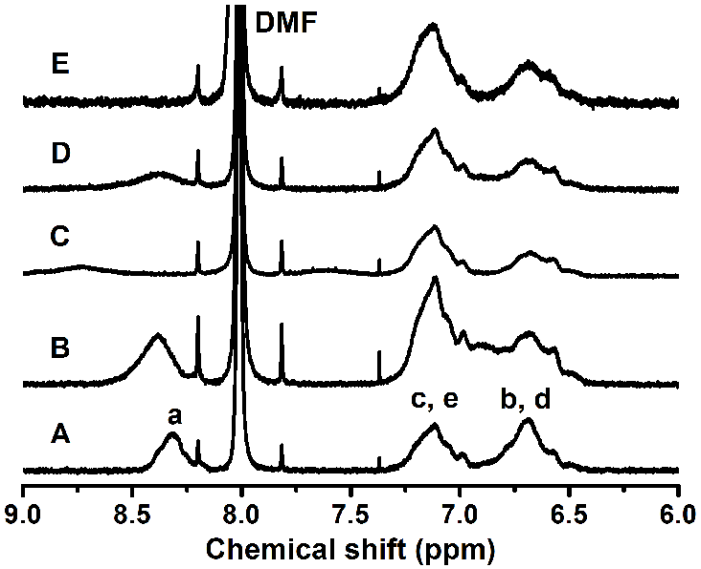

Fig. S1 ^{1}H NMR spectra of (A) PS_{94}-*b*-$P4VP_{95}$, HPW/BC composites with (B) r = 12 and (C) r = 2, and HSiW/BC composites with (D) r = 16 and (E) r = 2 in DMF-d_7.

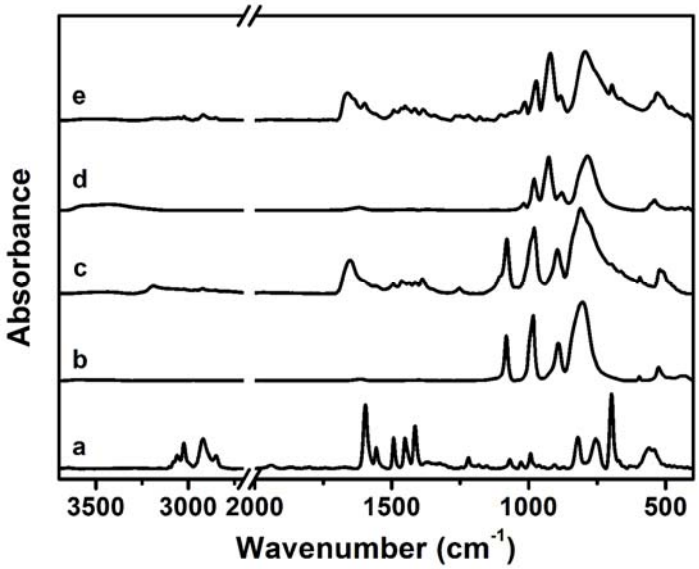

Fig. S2 IR spectra of (a) PS_{94}-*b*-$P4VP_{95}$, (b) HPW, (c) HPW/BC, (d) HSiW, and (e) HSiW/BC.

Table S1 Assignment of the characteristic vibration peaks of the POMs in FT-IR spectra of HPW, HPW/BC, HSiW, and HSiW/BC.[a]

Wavenumber (cm^{-1})				Assignment
HPW	HPW/BC	HSiW	HSiW/BC	
1082	1079	926	920	M–O_a asymmetric stretching
984	980	980	973	W–O_d asymmetric stretching
891	895	880	883	W–O_b–W asymmetric stretching
805	810	785	794	W–O_c–W asymmetric stretching

[a]O_a is the central oxygen, O_b the bridging oxygen that links two corner-sharing octahedra, O_c the bridging oxygen that links two edge-sharing octahedra, and O_d the terminal oxygen. M is P (for HPW and HPW/BC) or Si (for HSiW and HSiW/BC).

After removing the DMF in the solution under the reduced pressure, we got the samples of the BC–POM composites for the IR measurement. As shown in Fig. S2 and Table S1, the spectra of the BC–POM composites show the characteristic peaks of POMs

which are coincident with those in the spectra of pure POMs, indicating the chemical structures of HPW and HSiW are maintained in the micellization.

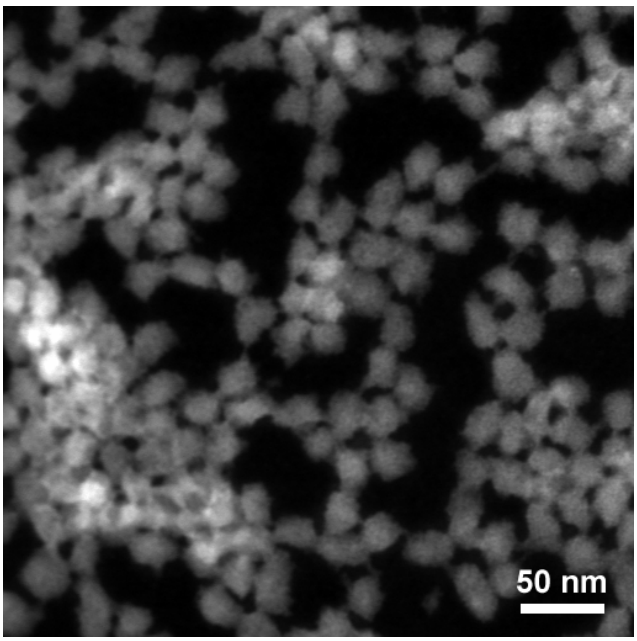

Fig. S3 HAADF-STEM image of spherical micelles of HPW/BC composites with r = 3.

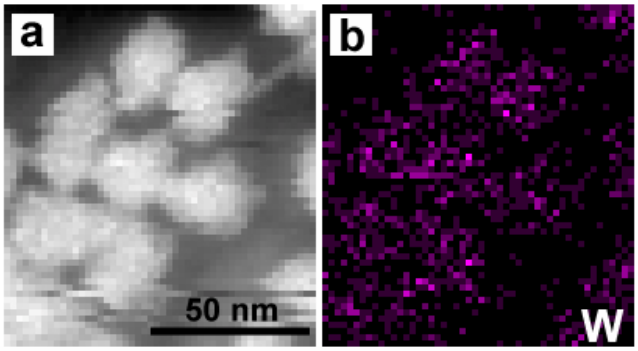

Fig. S4 (a) High magnification HAADF-STEM image and (b) corresponding elemental mapping images of spherical micelles of HPW/BC composites with r = 3.

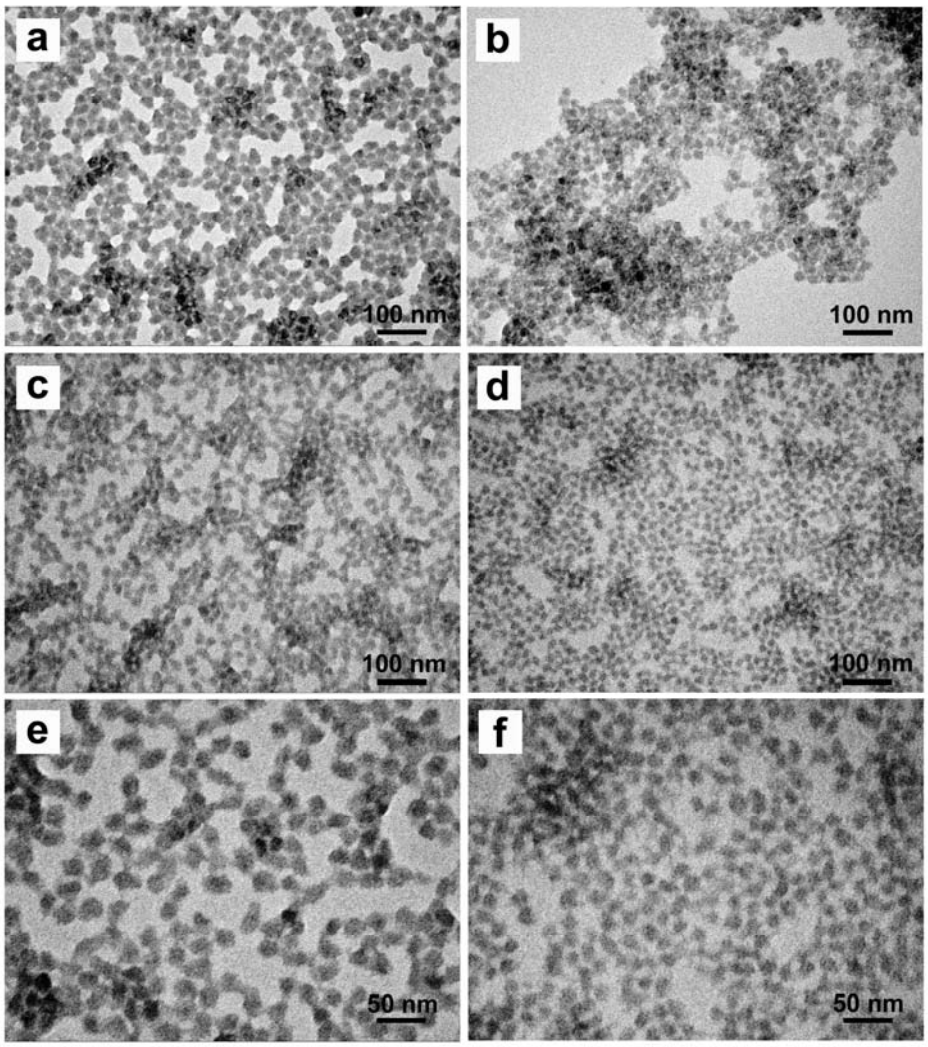

Fig. S5 TEM images of spherical micelles of HPW/BC composites with (a) r = 1, (b) r = 2, (c, e) r = 3, and (d, f) r = 6.

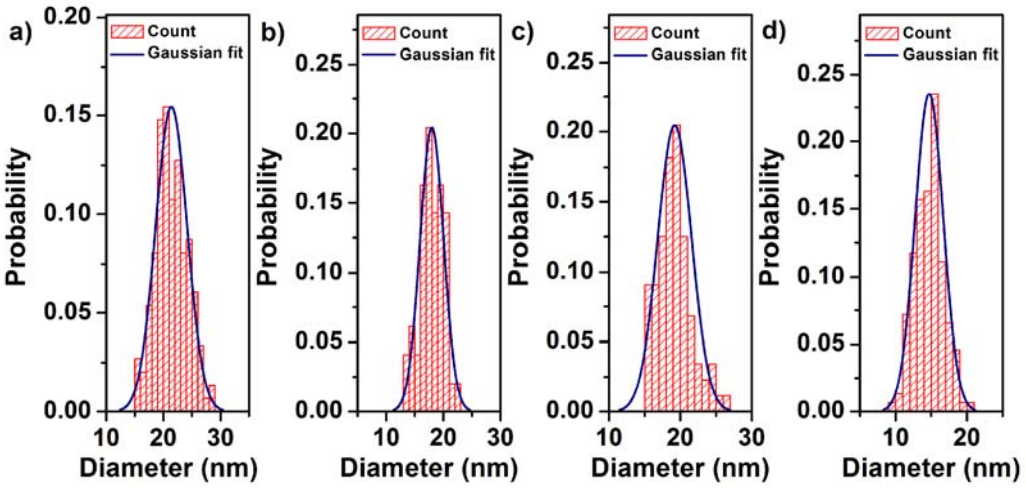

Fig. S6 Histograms and Gaussian fit curves of the core diameters of HPW/BC micelles with different *r*: (a) 1; (b) 2; (c) 3; (d) 6.

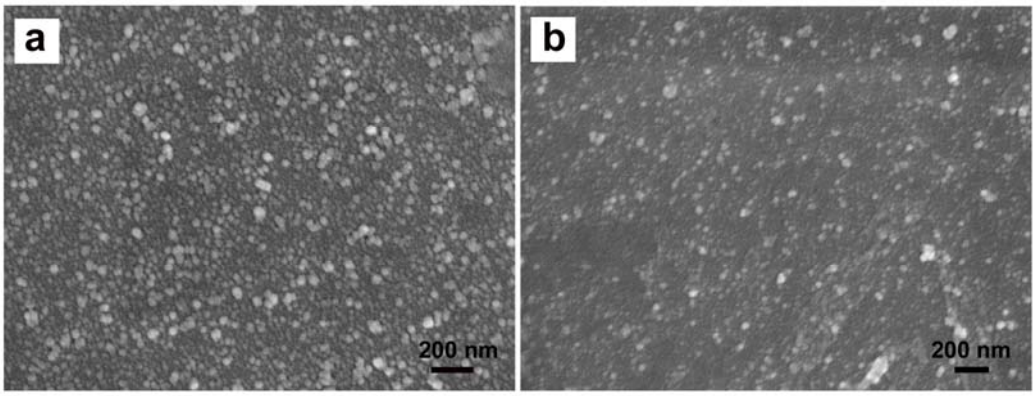

Fig. S7 SEM images of spherical micelles of HPW/BC composites with (a) r = 2 and (b) r = 3.

Except for the spherical micelles most of which are close to each other, there are also many big spheres which may derive from the aggregation of the spherical micelles during the sample preparation. The measured micellar diameters for both r = 2 and 3 are about 30 nm, which are bigger than the values measured by TEM (Fig. S5, S6) due to the additional PS coronas that are visible in the SEM investigation. So we can calculate out the thickness of the coronas which are 5–6 nm. The thickness values are smaller than the unperturbed end-to-end distance of the PS block (R_0) of 6.6 nm.

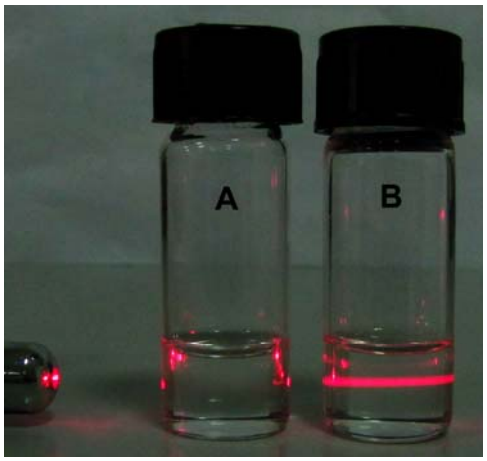

Fig. S8 Photograph of the solutions of HPW/BC composites with (A) r = 12 showing no Tyndall scattering and (B) r = 1 showing Tyndall scattering. This photograph is given as an example to illustrate that the solutions containing micelles show Tyndall scattering clearly, whereas the ones in which no aggregates are observed do not show the scattering.

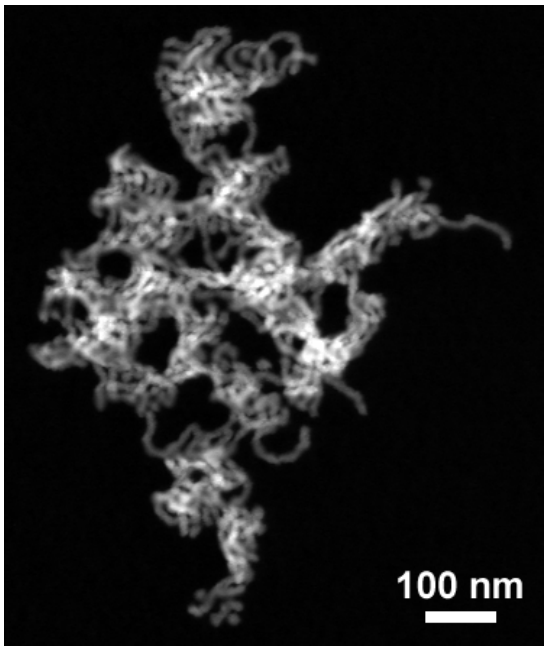

Fig. S9 HAADF-STEM image of wormlike micelles of HSiW/BC composites with r = 2.

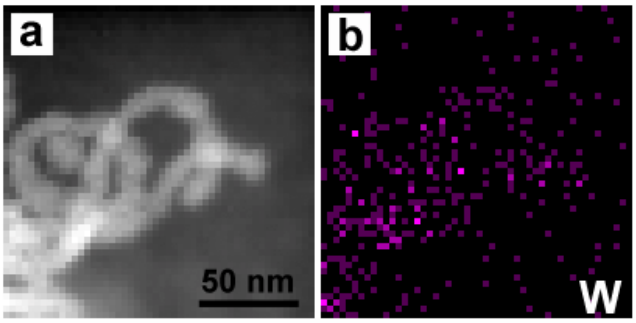

Fig. S10 (a) High magnification HAADF-STEM image and (b) corresponding elemental mapping images of wormlike micelles of HSiW/BC composites with r = 2.

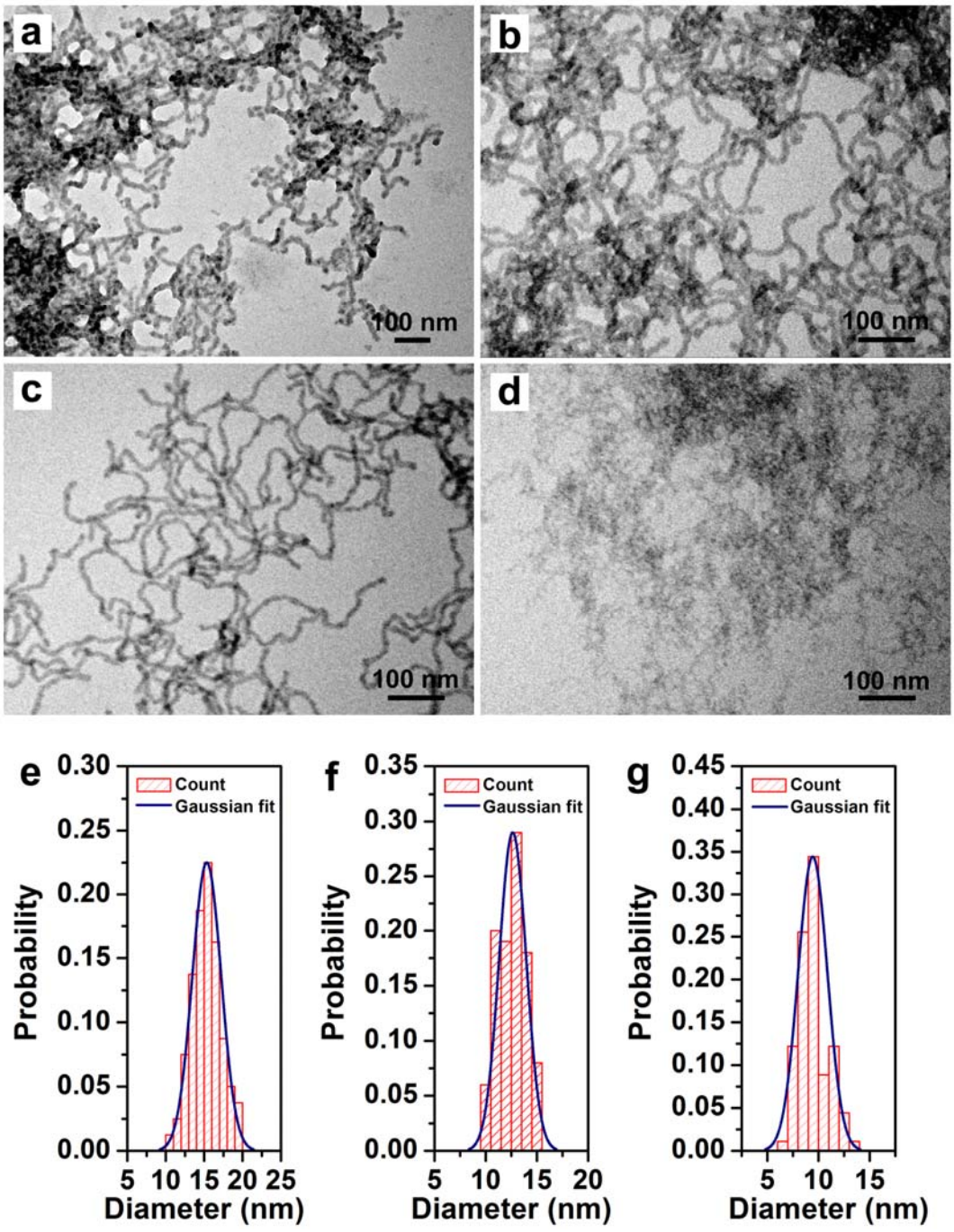

Fig. S11 TEM images of wormlike micelles of HSiW/BC composites with (a) r = 1, (b) r = 2, (c) r = 4, and (d) r = 8. The images (e), (f), and (g) are the corresponding histograms and Gaussian fit curves of the core diameters of the micelles for r = 1, 2, and 4, respectively. When r is 8, only a few irregular aggregates as shown in Fig. S11d were observed.

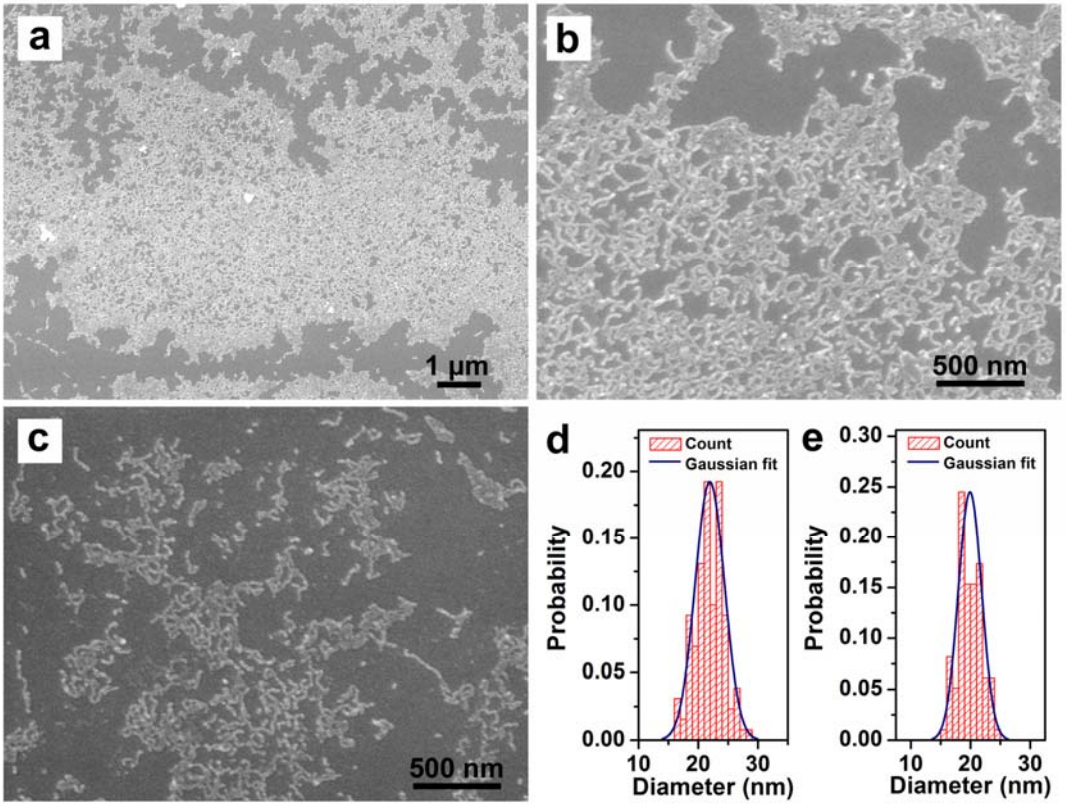

Fig. S12 SEM images of wormlike micelles of HSiW/BC composites with (a, b) r = 2 and (c) r = 4. The images (d) and (e) are the corresponding histograms and Gaussian fit curves of the micellar diameters for r = 2 and 4, respectively.

According to the SEM results, the measured micellar diameters for r = 2 and 4 are (21.9 ± 2.5) and (19.9 ± 1.9) nm, respectively, which are bigger than the values measured by TEM (Fig. S11) due to the additional PS coronas that are visible in the SEM investigation. So we can calculate out the thickness of the coronas which are 4.7 nm for r = 2 and 5.3 nm for r = 4, respectively. Both thickness values are smaller than the unperturbed end-to-end distance of the PS block (R_0) of 6.6 nm.

Packing parameters of composite micelles.

The fraction of the volume (f) is calculated by the following equations:

$$V_{PS} = M_{PS}/(N_A D_{PS}) \quad (1),$$

$$V_{P4VP} = M_{P4VP}/(N_A D_{P4VP}) \quad (2),$$

$$f_{P4VP} = V_{P4VP}/(V_{PS} + V_{P4VP}) \quad (3),$$

where V, M, and D are the volume, molecular weight, and density of the block marked by subscripts, respectively. N_A is the Avogadro's number ($N_A = 6.02\times10^{23}$). D_{PS} is 1.04–1.065 g/cm^3 (for amorphous PS), whereas D_{P4VP} is 1.114 g/cm^3.[2] For PS_{94}-*b*-$P4VP_{95}$, the fraction of the volume of the P4VP block (f_{P4VP}) is 0.51.

The average solvophobic volume per BC–POM composite (V_s, which does not include the volume of the solvent in the micellar core) is calculated by

$$V_s = V_{P4VP} + 95V_{POM}/r \quad (4),$$

where V_{POM} is the volume of a POM cluster (V_{POM} = 0.589 nm^3),[3,4] and r is the molar ratio of pyridine groups in PS_{94}-*b*-$P4VP_{95}$ to POMs. The fraction of the solvophobic volume in the composites (f_s) is calculated by

$$f_s = V_s/(V_s + V_{PS}) \quad (5).$$

The weight fraction of POMs in the BC–POM composites (W_{POM}) is given by

$$W_{POM} = m_{POM}/(m_{POM} + m_{BC}) \quad (6),$$

where m_{POM} and m_{BC} are the weight of POM and PS_{94}-*b*-$P4VP_{95}$ added in the preparation of the composites, respectively.

The stretching degree of the core blocks in the composite micelles (S_c) is calculated by

$$S_c = d_c/(2L_{P4VP}) \quad (7),$$

where d_c is the core diameter of the composite micelles measured through TEM, and L_{P4VP} is the contour length of P4VP blocks. The contour length of P4VP blocks (L_{P4VP}) is 23.8 nm ($L_{P4VP} = m\times0.25$ nm, where m is the degree of polymerization of the P4VP block).[4] In addition, the unperturbed end-to-end distance of the PS block (R_0) is 6.6 nm ($R_0 = 0.067M_{PS}^{0.5}$).[5]

References

(1) Lefèvre, N.; Fustin, C.-A.; Varshney, S. K.; Gohy, J.-F. *Polymer* **2007**, *48*, 2306–2311.

(2) Ko, J. H. *Polymer Data Handbook*; Oxford University Press: Oxford, **1999**.

(3) Rocchiccioli-Deltcheff, C.; Fournier, M.; Franck, R.; Thouvenot, R. *Inorg. Chem.* **1983**, *22*, 207–216.

(4) Bu, W. F.; Uchida, S.; Mizuno, N. *Angew. Chem., Int. Ed.* **2009**, *48*, 8281–8284.

(5) Yu, K.; Bartels, C.; Eisenberg, A. *Langmuir* **1999**, *15*, 7157–7167.